Measurement of electron capture and ionization cross sections for D_2 in collision with fast O^{8+} ions

S. Cheng and C. L. Cocke

J. R. Macdonald Laboratory, Department of Physics, Kansas State University, Manhattan, Kansas 66506

E. Y. Kamber

Department of Physics, Western Michigan University, Kalamazoo, Michigan 49008-3899

C. C. Hsu

J. R. Macdonald Laboratory, Department of Physics, Kansas State University, Manhattan, Kansas 66506

S. L. Varghese

Department of Physics, University of South Alabama, Mobile, Alabama 36688

We have measured cross sections for single capture, transfer ionization, single ionization, double ionization, ionization excitation, and transfer excitation for fully stripped oxygen projectiles at energies between 8 and 20 MeV on D_2 molecular targets. Coincidences between charge-analyzed projectiles and recoil D^+ and D_2^+ products were measured. The time of flight (TOF) of the recoil, collected by applying an extraction electric field, was used to separate the D^+ from D_2^+ ions. TOF spectra taken with no field were used to distinguish the D^+ ions from different dissociative channels, including the electronically excited $2p\sigma_u, 2s\sigma_g, 2p\pi_u$ channels and the double-ionization channel. The results are compared with two model calculations.

I. INTRODUCTION

Two-electron processes that occur when a fast charged particle impinges upon a multielectron target have been frequently studied in recent years. Since He is the simplest system for which such processes occur, much of this work has been done on He targets.[1-4] Two-electron transitions are driven both by independent interactions of individual target electrons with the projectile and by interactions between the electrons themselves following a single interaction of the projectile with one electron. The latter processes, which can be quite important for singly charged projectiles, are usually spoken of in terms of correlations present in initial or final target wave functions or induced during the collision itself, and include shakeoff, shakeup, and shakeover. When the projectile is highly charged, as is the case for the system studied in this paper, the former processes tend to dominate, and theoretical treatments can be realistically based on the independent-electron model. Several such treatments have appeared in the literature, including multiple expansion defined on one center (MEDOC, Gayet and Salin[5]), classical trajectory Monte Carlo (CTMC, Olson[6]) and the close-coupling method (Janev and Presnyakov[7]).

In this paper we examine one- and two-electron processes that occur when a fast bare nucleus of oxygen is incident on a molecular deuterium target. The choice of the simplest two-electron molecule as a target has the advantage that any two-electron transition results in a dissociative state of the molecule, and the detection of the ionic products allows the extraction of information on the angular orientation of the molecule at the time of the collision. It also allows us to use the energies of the ionic products to distinguish among the various excited molecular ions formed in the collision, and to separate simultaneous ionization and excitation from double ionization for example. We are thus able to extract separate cross sections for double ionization and for ionization excitation. Such a separation, not possible for He targets, allows a more detailed comparison to be made between experiment and theory.

We report here total cross sections for one- and two-electron transitions which occur when 8–20-MeV O^{8+} ions collide with molecular deuterium. Coincidences between charge-selected recoil and projectile ions were used to extract separate cross sections for events in which D^+ and D_2^+ ions were produced. Analysis of the energies of the D^+ ions was used to deduce separate cross sections for ionization excitation and double ionization channels accompanying either direct ionization of the molecule or capture from the molecule.

II. EXPERIMENT

The experimental apparatus is shown in Fig. 1. The incoming O^{8+} beam was collimated by two successive four-jaw slits S and was cleaned by a magnet $M1$ before being focused into the collision region. The charge purity of the beam at this point is very important to the results of the experiment because the capture cross sections for O^{8+} on D_2 are several orders of magnitude less than the ionization cross section. Thus even a small charge state
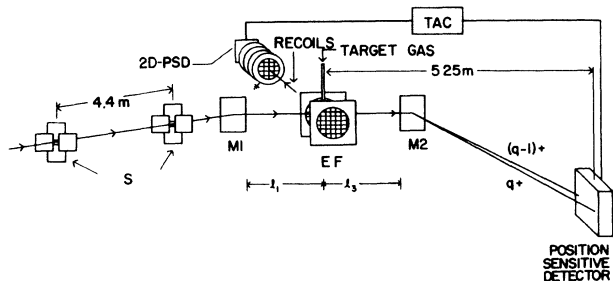
FIG. 1. Schematic of apparatus. S denotes adjustable slits, EF is the extraction field, 2D-PSD is the two-dimensional position-sensitive detector, and $M1$, $M2$ are magnets.

impurity in the beam can give rise to coincidences between O^{7+} ions and D_2^+ or D^+ ions formed by simple ionization which are not caused by true capture from the D_2 target. A small O^{7+} impurity is easy to come by, since the cross section for capture from the residual gas is several orders of magnitude larger than that for capture from molecular deuterium. At the collision region, D_2 gas of a few mTorr pressure was blown at right angles to and 2 mm above the beam through a multicapillary tube jet made from a broken channel plate. The D^+ and D_2^+ ions produced were extracted toward a two-dimensional position-sensitive backgammon anode detector (2D-PSD) which was mounted at 90° to the beam direction and was 97.7±1.0 mm from the jet. After passing through the collision region, the beam was deflected by a magnet $M2$ to separate O^{8+} from O^{7+} and was detected by a one-dimensional position-sensitive solid-state detector (PSD). The timing signal from the PSD was used to start the TAC (time-to-amplitude converter) and that from the 2D-PSD to stop a TAC. A D_2 gas target was chosen instead of H_2 to avoid contamination of the H^+ peak by protons collisionally liberated from the residual gas. An aperture of 6-mm diameter was placed between the jet and the detector to restrict the view of the detector to only the central collision region. In order to get a sufficiently large timing signal, signals from the back of both the first and the second channel plates were summed and used to stop the TAC. The relative efficiency for the detection of D^+ and D_2^+ ions was found to be independent of the velocity of these ions for sufficiently high ion energies into the channel plates and sufficiently low discriminator settings, and the efficiency was therefore taken to be the same for these two ionic species. The extraction voltage was about 1000 V to ensure that every ion, including D^+ ions whose dissociation energy might potentially throw them outside the spatial range covered by the 2D-PSD, would be collected.

III. DATA ANALYSIS

A. The data

A typical coincidence spectrum and its projections are shown in Fig. 2. The time of flight of the recoil ions al-
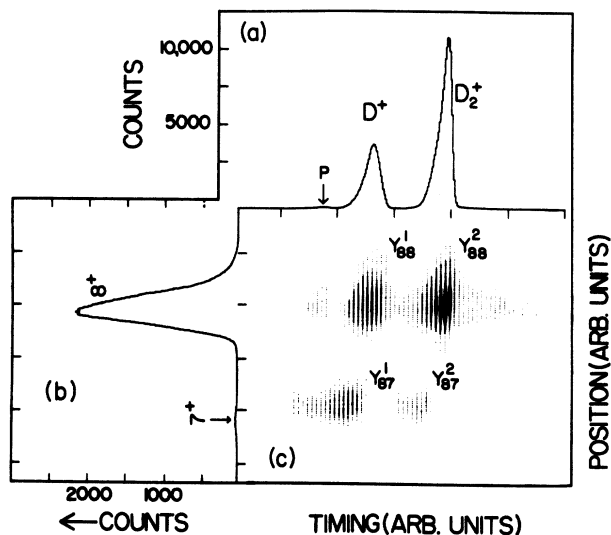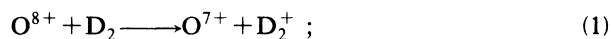

FIG. 2. A typical coincident spectrum and its projections. (a) Time-of-flight spectrum of coincident D^+ and D_2^+. (b) Position spectrum of the projectiles. (c) Two-dimensional spectrum.
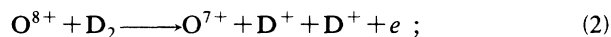
lows the identification of groups from D_2^+, D^+, and H^+ ions. The last of these is created by ionization of the residual gas. From previous experience with this apparatus, we have determined that the contamination of the D^+ peak by H_2^+ ions is negligible. Coincident events located at islands Y_{88}^1, Y_{88}^2, Y_{87}^1, Y_{87}^2 are proportional to the relative cross sections for ionization and capture collisions in which D_2^+ and D^+ are created. Notice that, in the spectrum of Fig. 2, the time spectrum in coincidence with O^{7+} is shifted relative to that in coincidence with O^{8+}. This is due to the fact that projectiles of different charge state hit the PSD at different places, and the charge collection time in the PSD is dependent on the location of the ionizing event.

From the yields in these islands, with additional information as discussed below, we extract six separate cross sections corresponding to the following six processes:
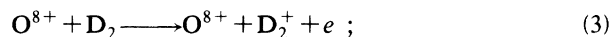
Single capture (SC),

$$O^{8+} + D_2 \longrightarrow O^{7+} + D_2^+ ; \tag{1}$$

transfer ionization (TI),

$$O^{8+} + D_2 \longrightarrow O^{7+} + D^+ + D^+ + e ; \tag{2}$$

single ionization (SI),

$$O^{8+} + D_2 \longrightarrow O^{8+} + D_2^+ + e ; \tag{3}$$

double ionization (DI),

$$O^{8+} + D_2 \longrightarrow O^{8+} + D^+ + D^+ + 2e ; \tag{4}$$

transfer excitation (TE),

$$O^{8+} + D_2 \longrightarrow O^{7+} + (D_2^+)^* \rightarrow D + D^+ ; \tag{5}$$

ionization excitation (IE),

$$O^{8+} + D_2 \longrightarrow O^{8+} + (D_2^+)^* + e \rightarrow D + D^+ + e . \tag{6}$$
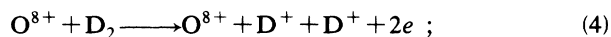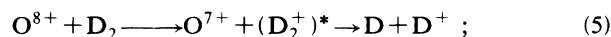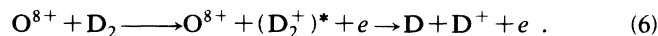
The asterisk indicates that the D_2^+ molecule is electronically excited, and will always give rise to dissociation of the molecule. Double capture was experimentally determined to be immeasurably small over our projectile velocity range. Double excitation would (a) give rise to two neutral fragments, (b) autoionize to a bound singly ionized molecule, or (c) dissociate into a charged ion and a neutral fragment. Products from channel (a) would go undetected in our experiment, while those from channel (b) would be masked by the much larger direct processes from production of D_2^+. Channel (c) would appear as "ionization-excitation" in our experiment, but should be much weaker than channel (b)[8-10]. The extraction of six cross sections from the four areas requires that the production of the D^+ ions be further separated into events in which a single D^+ ion is created and those for which two D^+ ions are created. This separation is not only desirable but necessary to the interpretation of any of the D^+ data, since the probability per collision for detecting a D^+ is approximately a factor of two larger for the double ionization case. The data must be further corrected for substantial double collision contributions to the Y_{87}^i islands ($i=1,2$).

B. Corrections for double collisions

The yield of events in each of the islands in Fig. 2 is influenced by double collisions in which the O^{8+} captures a single electron in the residual gas or the target gas in one collision and ionizes the D_2 target in a second collision. The details of the correction are quite lengthy and complicated and are described in Appendix A, but we give a summary here. Since the cross section for ionization of D_2 by either O^{7+} or O^{8+} is two to three orders of magnitude larger than that for capture from D_2, an O^{7+} contamination in the O^{8+} beam of a few parts per thousand is sufficient to give a double collision yield of contaminant events, which result in the detection of O^{7+} ions coincidence with a recoil ion, comparable to that which comes from a true capture in a single collision. To first approximation, the double-collision contributions to the Y_{87}^1, Y_{87}^2 islands are given by the product of the number of counts in the Y_{88}^1, Y_{88}^2 islands multiplied by the mean charge state impurity

$$f = \frac{\mathscr{Y}(O^{7+})}{\mathscr{Y}(O^{8+})} \, , \tag{7}$$

where $\mathscr{Y}(x)$ is the yield of x.

A typical fraction of f in our beamline was about 1 part in 2000, with a background pressure of 10^{-7} mTorr and an energy of 1 MeV/amu. The actual correction made was based on the analysis of the system in terms of three charge exchange regions: before, at, and after the collision region. The major correction is for the Y_{87}^2 island, from which a double collision contribution as high as one-third of the raw yield must be subtracted. The correction in the ionization channels is negligible.

C. Identification of the dissociation channels

When a D_2^+ molecule is created in either a simple ionization or a capture collision, there is a substantial probability that the remaining electron will be electronically excited. All electronically excited states of D_2^+ dissociate, yielding D^+ ions. However, D^+ ions may also come from the doubly ionized molecule D_2^{2+} which dissociates into $D^+ + D^+$. Since the efficiency to detect an event in which one D^+ is created is different from that to detect an event in which two D^+ ions are created, we have to separate the $D^+ + D^+$ channel from the $D^+ + D$ channel in order to interpret the data correctly. This separation was performed by using the energy spectra of the ionic D^+ fragments produced in the dissociation process. The technique has been used previously and discussed in detail by Wood et al. and other authors.[11-17] Figure 3(a) shows the relevant potential energy curves for the main dissociative channels of D_2^+ involved. Because the initial vibrational state of the D_2 molecule represents a distribution in internuclear distances, Frank-Condon transition to a dissociative potential curve will produce a reflected spread in the energy of the dissociation frag-
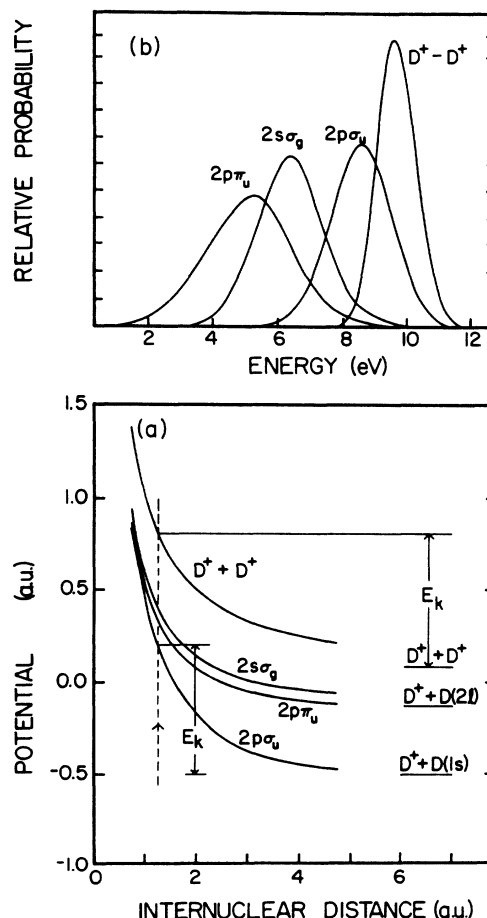

FIG. 3. (a) The potential curve of a D_2 molecular ion. The mean released kinetic energy E_k is shown for the $2p\sigma_u$ and $D^+ + D^+$ channels. (b) Calculated kinetic energy distributions of $2p\sigma_u$, $2s\sigma_g$, $2p\pi_u$, and double-ionization channels.

ments. Wood[18] has used a quantum-mechanical calculation as well as the reflection approximation to calculate the expected energy distributions for a H_2 target and concluded that the differences are extremely small. We have used the reflection approximation to calculate the expect-
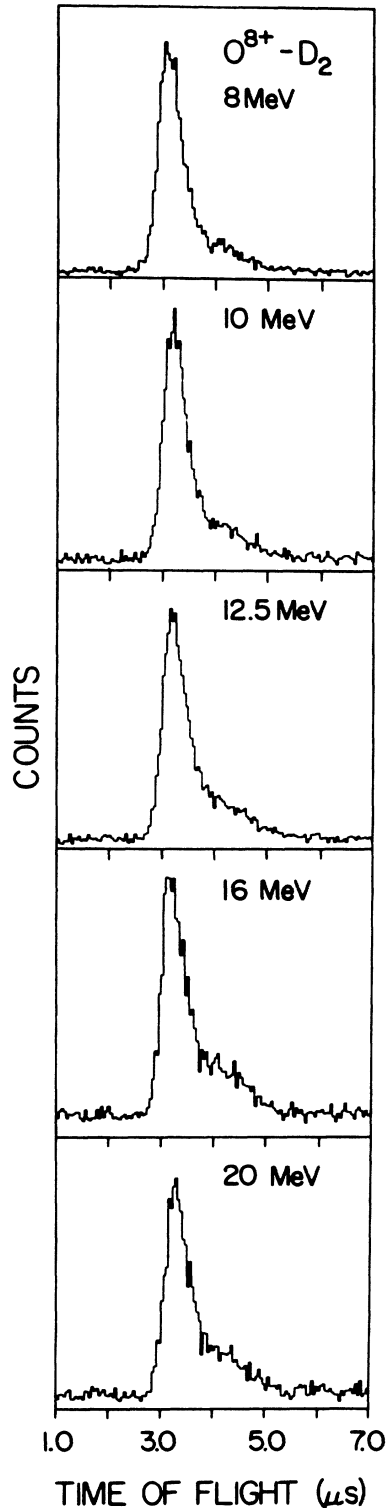

FIG. 4. Typical time-of-flight spectra for D^+ ions coincident with O^{8+} of energies 8–20 MeV.

ed distributions for the $2p\sigma_u$, $2s\sigma_g$, $2p\pi_u$, and D^+-D^+ channels from a D_2 target and show the results in Fig. 3(b). The experimental spectra were obtained by measuring time-of-flight spectra of the D^+ ions with no extraction field in coincidence with O^{8+} and O^{7+} for impact energies from 8 to 20 MeV. Figure 4 shows the spectra obtained in coincidence with O^{8+}. An absolute velocity scale was established by calibration of the TAC time scale and careful measurement of the target-detector distance. These spectra were background subtracted and converted to kinetic energy spectra and were normalized such that the area enclosed by each spectrum was unity. The resulting experimental energy spectrum was considered to be a superposition of four possible energy distributions, corresponding to the production of D_2^{2+}, $2p\sigma_u$, $2s\sigma_g$, and $2p\pi_u$. A linear least-squares fitting program was used to fit the experimental spectra to a sum of the distributions shown in Fig. 3(b). Figure 5 shows an example of the results of the fitting process, and the fractional areas of each of the four contribution channels are shown in Tables I and II. Further data reduction details are given in Appendix A.

IV. RESULTS AND DISCUSSION

The relative cross sections obtained as described above and in Appendix A were placed on an absolute scale [N, in Eq. (A7)–(A12)] by normalizing our total capture cross section ($\sigma_{TC}=\sigma_{SC}+\sigma_{TI}+\sigma_{TE}$) for 8-MeV O^{8+} on D_2 to the total capture cross section for the same system measured by Sanders.[19] The final results are tabulated in Table III. The error bars in Table III come from two contributions. One is from uncertainties of the fractions in Tables I and II. These fractions enter into the calculation of all cross sections, and thus the error bars on these fractions will be reflected in the results of the calculated cross sections. To evaluate the cross section errors from this source, we calculated cross sections for a given run
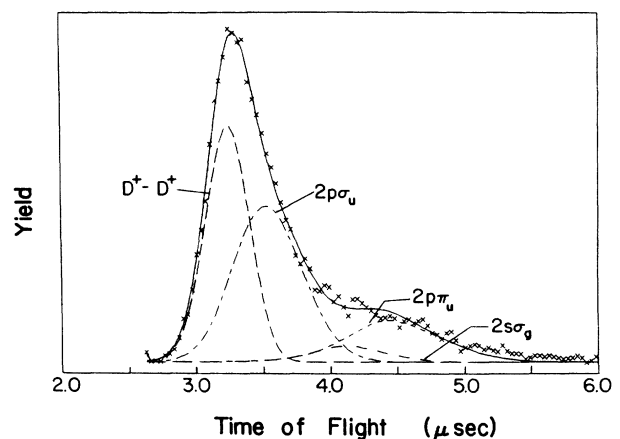

FIG. 5. Experimental data from Fig. 4 and the fitted curve at 12.5 MeV. The crosses are the experimental data, the solid line is the fitted curve, and the dashes are the contributions from individual channels, as indicated in the figure.

CHENG, COCKE, KAMBER, HSU, AND VARGHESE

TABLE I. Fractions of D^+ yield from different channels in coincidence with O^{8+}.

Energy (MeV)	D^+D^+	$2p\sigma_u$	$2s\sigma_g$	$2p\pi_u$
8	0.49±0.06	0.34±0.04	0.05±0.02	0.12±0.02
10	0.44±0.06	0.39±0.05	0.04±0.02	0.13±0.02
12.5	0.38±0.05	0.41±0.06	0.05±0.02	0.16±0.02
16	0.36±0.05	0.42±0.06	0.06±0.02	0.16±0.02
20	0.30±0.04	0.46±0.06	0.05±0.02	0.19±0.02

by varying the fractions in Tables I and II from their upper to lower limits. The deviations of the resulting cross sections due to the variation of these fractions were designated as e_1. The second contribution includes random errors in counting statistics, relative gas pressure measurement, and background level determination, all of which are reflected in the reproducibility of the results. We dealt with this contribution by taking the mean fractions in Tables I and II to calculate the cross sections of repeated runs at a given energy. The standard deviation of the mean cross section was noted as e_2. Approximately considering these two contributions as uncorrelated, we combined two deviations quadratically by using the formula $e = (e_1^2 + e_2^2)^{1/2}$ to get the final relative error bars, which are given in Table III. In addition, there is an overall uncertainty of 15% in the absolute normalization.

In Figs. 6 and 7, we plot all cross sections we measured as a function of impact ion energy. The single capture cross section falls off rapidly when the bombarding energy increases while the single ionization cross section stays flat over a wide energy range (8–16 MeV) and then falls off. These features also are reflected in the cross sections involving two-electron processes. In an independent electron model, the cross section for a two-electron process can be written in terms of the b-dependent probabilities for the corresponding one-electron processes. Taking transfer ionization as an example (generalization to other cases is evident), this gives

$$\sigma_{TI} = 2\pi \int 2P_C(b)P_I(b)b \, db \, , \qquad (8)$$

where P_C and P_I are single-electron capture and ionization probabilities, respectively. By forming the ratio $\sigma_{TI}/\sigma_{TC} = \int P_C(b)P_I(b)b \, db / \int P_C(b)b \, db$, one obtains a weighted average $\bar{P}_I$ over an impact parameter range

given by the requirement that capture occurs. One expects P_C to be concentrated at much smaller b than P_I for these collisions, and thus one can evaluate an average probability for ionization and excitation "at small b" from the ratios σ_{TI}/σ_{TC} and σ_{TE}/σ_{TC}. Similarly, the corresponding average probability for ionization and excitation "at large b" are given by the ratios σ_{DI}/σ_I and σ_{IE}/σ_I ($\sigma_I = \sigma_{SI} + \sigma_{IE} + \sigma_{DI}$, total ionization). Some qualitative interpretation of the trends of these weighted-average probabilities can be made from our data. In Fig. 8 we plot the ratio of the cross section for each of these two-electron processes to that for the related one-electron process. For energies between 8 and 20 MeV, the ratio of σ_{TI} to total capture σ_{TC} is consistently larger than the ratio of σ_{DI} to total ionization σ_I. Thus the impact parameter averaged probability to ionize an electron is bigger at small b than at large b, as would be expected. A similar situation exists in the case of exciting the second electron. For excitation an interesting feature is revealed by the near energy independence of the σ_{IE}/σ_I and σ_{TE}/σ_{TC} ratios in Fig. 8. It appears that the average probability for electronically exciting an electron is not particularly sensitive to bombarding energy for large $b(\sigma_{IE}/\sigma_I)$ or small $b(\sigma_{TE}/\sigma_{TC})$. Indeed, it is only a factor of about 2 larger for σ_{TE} than for σ_{IE}. This is in contrast to the case for the average probability for ionization, given by the σ_{TI}/σ_{TC} and σ_{DI}/σ_I ratios in Fig. 8, where this probability is seen to decrease rapidly with increasing energy and to be nearly an order of magnitude smaller for small b. The general conclusion to be drawn is that the greater the ionizing power of the projectile (slow moving or small b), the more important the ionization process is compared to the excitation. We are not aware of any observation of this feature in previous experimental or theoretical work.

We can compare our results with the results of two

TABLE II. Fractions of D^+ yield from different channels in coincidence with O^{7+}.

Energy (MeV)	D^+D^+	$2p\sigma_u$	$2s\sigma_g$	$2p\pi_u$
8	0.74±0.05	0.14±0.03	0.05±0.02	0.07±0.03
10	0.68±0.05	0.16±0.04	0.06±0.02	0.10±0.03
12.5	0.61±0.04	0.18±0.04	0.08±0.02	0.13±0.03
16	0.56±0.04	0.21±0.04	0.08±0.03	0.15±0.05
20	0.45±0.04	0.23±0.05	0.06±0.03	0.26±0.05

TABLE III. Cross sections (in units of 10^{-18} cm^2) for O^{8+} on D_2 at energies 8–20 MeV. The error bars given for these cross sections do not include the absolute overall normalization uncertainty of 15%.

E (MeV)	SC	TI	SI	DI	total	TE 2pσ_u	TE 2sσ_g	TE 2pπ_u	TE total	IE 2pσ_u	IE 2sσ_g	IE 2pπ_u
8	3.8 ±0.42	5.7 ±0.45	1250 ±19	148 ±19	3.72 ±0.72	2.0	0.72	1.0	286 ±34	191	28	67
10	1.9 ±0.18	2.0 ±0.20	1300 ±27	119 ±16	1.8 ±0.31	0.90	0.34	0.56	281 ±33	196	20	65
12.5	0.74 ±0.10	0.68 ±0.06	1350 ±28	89 ±10	0.81 ±0.10	0.37	0.17	0.27	271 ±22	179	22	70
16	0.45 ±0.05	0.25 ±0.03	1240 ±26	66 ±9.0	0.36 ±0.04	0.17	0.066	0.12	220 ±18	144	21	55
20	0.12 ±0.01	0.043 ±0.005	970 ±9.0	37 ±5.0	0.098 ±0.011	0.041	0.011	0.046	159 ±10	105	11	43

theoretical calculations.[20,21] Shingal[20] used a simple model in which a D_2 molecule was described as an atom with two independent electrons. The effective charge of this model atom was adjusted such that the binding energy of the outer electron was the same as that in the D_2 molecule. A multistate semiclassical impact parameter method[22] was then used to perform the calculation. Single-electron transition probabilities were calculated

and two-electron transition probabilities were evaluated using products of these probabilities as discussed earlier. His results are shown in Table IV. Meng, Reinhold, and Olson[21] used the CTMC method to calculate the cross sections for our system. The results are shown in Table IV also. Generally, both calculations are in fairly good agreement with our experiment results. For the strongly populated channel, i.e., the single ionization channel, both models give fair agreement. The agreement between the experimental and theoretical results are poor for the σ_{TE}, σ_{TI}, σ_{IE}, and σ_{DI} channels taken separately, but are
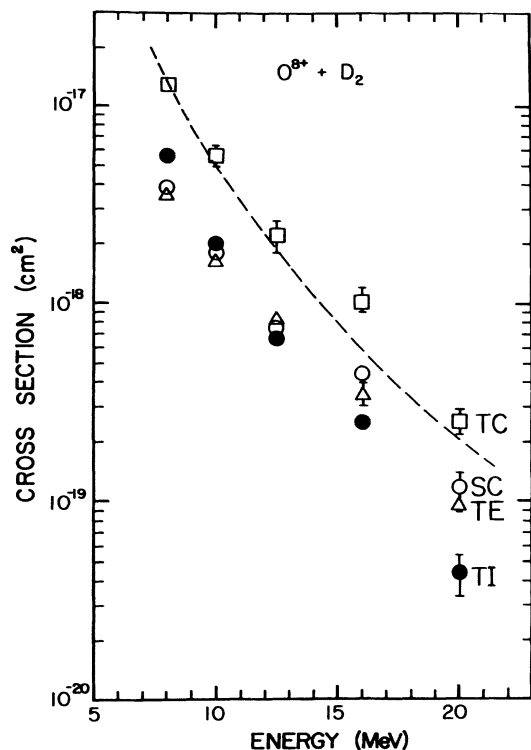

FIG. 6. Cross sections for O^{8+} on D_2. Open circle, single capture (SC); solid circle, transfer ionization (TI); open square, total capture (TC); dashed line, Ref. 19 (TC); open triangle, transfer excitation (TE).
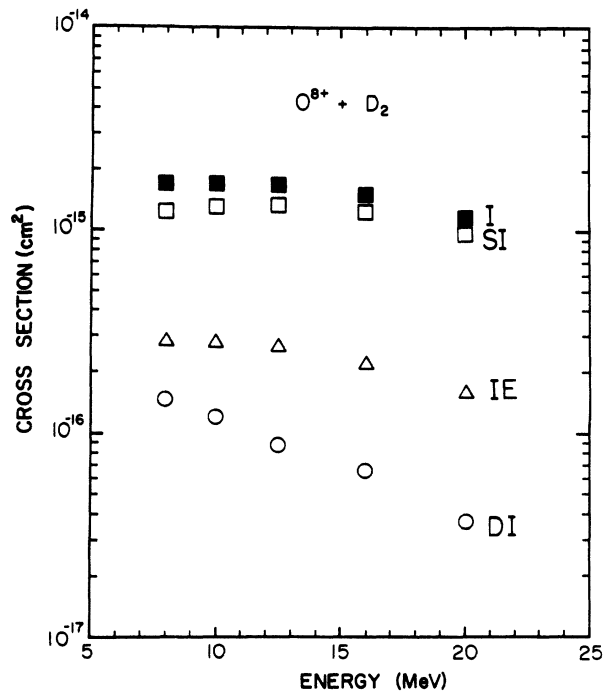

FIG. 7. Cross sections for O^{8+} on D_2. Solid square, total ionization (I); open square, single ionization (SI); open circle, double ionization (DI); open triangle, ionization excitation (IE).
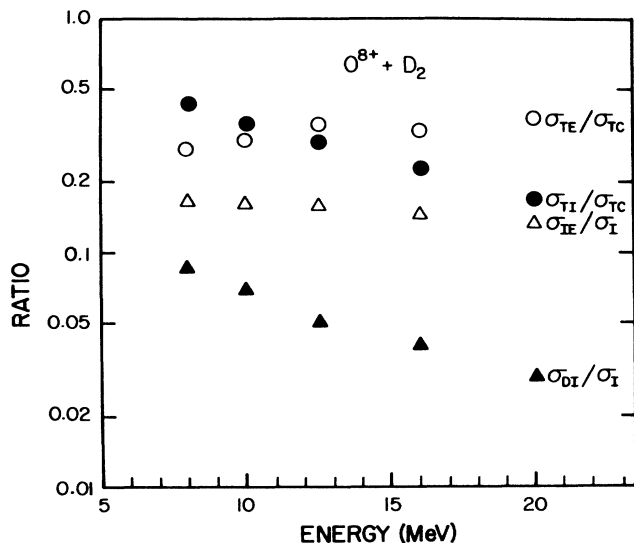
FIG. 8. Ratios of cross sections for O^{8+} on D_2. Open circle, transfer excitation over total capture $(\sigma_{TE}/\sigma_{TC})$; solid circle, transfer ionization over total capture $(\sigma_{TI}/\sigma_{TC})$; open triangle, ionization excitation over total ionization (σ_{IE}/σ_I); solid triangle, double ionization over total ionization (σ_{DI}/σ_I).

better if the ionization and excitation cross sections are summed (for example, $\sigma_{TE}+\sigma_{TI}$, $\sigma_{IE}+\sigma_{DI}$). Both calculations predict that excitation is consistently weaker than ionization, while the experiment indicates that excitation is about to have the same order of magnitude as ionization at small b and is the stronger process at large b.

V. CONCLUSION AND SUMMARY

The major features of the cross sections we have measured for one- and two-electron capture, excitation and ionization, appear to be interpretable in terms of independent two-electron models. The experiment indicates that the probability for electronic excitation of the molecule by an O^{8+} projectile in our energy range is large and remarkably weakly dependent on either projectile energy or impact parameter. Model calculations which otherwise give fair agreement with our results do not seem to offer an explanation for this result.

The use of the molecular target allowed the experimental isolation of excitation channels, since ionic fragments are produced. These fragments contain information not only about final channel distributions, but also about the dependence of both one- and two-electron transition probabilities on the angle between the beam and the molecular axis. The present work, separating the channels in total cross section, is preliminary to studies of this molecular orientation effect.

ACKNOWLEDGMENTS

APPENDIX A: DATA REDUCTION

We describe here the procedure used to go from the raw measured yields $Y^i_{q,q'}$ from spectra such as that shown in Fig. 2 to the six cross sections deduced. The notation is that q is the projectile charge $(q=8)$, q' is the final projectile charge $(q'=8$ or $=7)$, and i, the mass in amu of the recoil ion, is 1 (D^+) or 2(D_2^+). The first step was to convert each yield into a yield per incident particle $y^i_{q,q'}$ by dividing the raw yield from each island by the

TABLE IV. Theoretical cross sections (in units of 10^{-18} cm^2) for O^{8+} on D_2 at energies 8–20 MeV.

E (MeV)	SC	TI	TE	SI	DI	IE	Note
8	1.74	4.1	1.0	1730	593	130	T^a
	1.77	13.6		1120	58.6		T^b
	3.8	5.7	3.72	1250	148	286	E^c
10				1144	478		T^b
				1300	119		E^c
12.5	0.66	1.2	0.21	1490	445	85.7	T^a
				930	406		T^b
	0.74	0.68	0.81	1350	89	271	E^c
16	0.68			811	315		T^b
	0.45			1240	66		E^c
20	0.35	0.37	0.086	1210	248	58.7	T^a
				714	260		T^b
	0.12	0.043	0.098	970	37	159	E^c

[a]Theory, Shingal (Ref. 20).
[b]Theory, Meng, Reinhold, and Olson (Ref. 21).
[c]Experiment, this work.

total number of beam particles incident on the target during the run, as determined from the PSD spectrum, and correcting for computer dead time. All further analysis is done in terms of the $y^i_{q,q'}$.

1. Double collision corrections

Only double collisions corresponding to electron capture in one collision and ionization of the D_2 gas in a second collision are important. We consider separately events for which the charge exchange occurs in the background gas before or after the collision chamber and those for which the charge exchange occurs with the D_2 gas in the collision chamber itself. This separation is necessary, since some of the double-collision events occurring in the latter case are masked by detection of the true single-collision products resulting from the capture part of the collision, and special consideration of the relevant detection efficiencies enter.

a. Capture outside the collision chamber

It can be readily shown that the double-collision yield, designated by $y^i_{8,7}$ (DCA), due to capture in the residual gas before the chamber followed by ionization of D_2, or ionization of D_2 followed by capture in the gas after the chamber is given by

$$y^i_{8,7}(DCA)=y^i_{8,8}F\beta , \tag{A1}$$

where F is the charge-state fraction of O^{7+} in the O^{8+} beam measured with no D_2 in the target chamber and β is the ratio of the weighted average of the cross section for ionization of D_2 by O^{7+} and O^{8+} to that for ionization by O^{8+} alone, and is close to unity. The weight of the O^{7+} cross section to that of the O^{8+} fraction is in the ratio of the distance traversed by the beam after the collision region to that before the collision region. Only distances between the magnets $M1$ and $M2$ in Fig. 1 enter. In our case, we estimated the ionization cross sections for O^{7+} and O^{8+} to be in the ratio of $(7/8)^2$,[23] resulting in a value for β of 0.85 for our geometry.

b. Capture in the collision chamber

The analysis is complicated by the fact that some of the double-collision events which result in charge exchange are not detected because the true ion coincidence yield from the charge-exchange collision is detected first. Thus a simple analysis in terms of charge state impurities is replaced by a more detailed analysis, which gives the following expressions for the double collision contributions caused by capture in D_2 in one collision and ionization of D_2 in another, designated by $y^i_{8,7}$ (DCB):

$$y^1_{8,7}(DCB)=\tfrac{1}{2}y^1_{8,8}\left[y^2_{8,7}\frac{1}{\epsilon_8}+y^1_{8,7}\frac{(1-\epsilon_7)}{\epsilon_7}\right] , \tag{A2}$$

$$y^2_{8,7}(DCB)=\tfrac{1}{2}y^2_{8,8}\left[y^1_{8,7}\frac{(1-\epsilon_y)}{\epsilon_7}+y^2_{8,7}\frac{(1-\epsilon)}{\epsilon}\right] . \tag{A3}$$

Here ϵ is the probability that a single D^+ or D_2^+ ion

created alone anywhere in the D_2 target will be registered by the channel plate detector. The average efficiency ϵ_8 is the probability that a collision of O^{8+} with D_2 producing an O^{8+} and one or more D^+ ions, (DI or IE, both of which contribute to the $Y^1_{8,8}$ island) will result in the detection of a D^+ ion. Because DI events give rise to two D^+ ions and IE gives rise to only one, ϵ_8 will depend on the relative cross sections for DI and IE, and thus the information deduced from the TOF spectra listed in Table I, along with ϵ, enter into the calculation of ϵ_8. It can be shown that ϵ_8 is given by

$$\epsilon_8=\frac{(2-\epsilon)+\beta_8}{(1+\beta_8)}\epsilon , \tag{A4}$$

where

$$\beta_8=\left|\frac{1}{F_8}-1\right|(2-\epsilon) , \tag{A5}$$

and F_8 is the fractional contribution of the D^+-D^+ channel in the TOF spectrum taken from the first column of Table I. For example, at 8 MeV, $F_8=0.49$. The efficiency ϵ_7, the weighted average detection efficiency for TI plus TE, is found from an identical expression with the subscript 8 replaced by 7, and F_7 taken from the first column of Table II.

Expressions in Eq. (A2) and (A3) are similar to that in (A1), and nearly have the form of a product of an ionization yield with the probability for capture in the target gas. The added complexity comes only because the detection of one recoil excludes the detection of others. In the limit as ϵ goes to zero, Eq. (A2) and (A3) revert to expressions resembling (A1), with the charge exchange fraction F replaced by one calculated from the measured capture probabilities in the D_2 gas.

The efficiency ϵ was determined by requiring that the increase of the O^{7+} charge-state fraction with D_2 pressure observed as single in the PSD agreed with that calculated from expressions (A2) and (A3). We found ϵ to be equal to 14%. This rather low value is attributed to several factors including the effective open area ratio of the channel plate, the transmission of three grids in front of this detector and exclusion of part of the D_2 target from the field of view of the detector in the region before and after the gas jet itself. We established experimentally that, for sufficiently high channel-plate voltage and low discriminator setting, the relative yields of D^+ and D_2^+ ions was independent of the energy of the ions striking the front channel plate, and thus believe the assumption of a single universal ϵ for both D^+ and D_2^+ is justified.

2. Cross-section determinations

The yield of each island was first corrected for double collision events to obtain corrected yields for each of the four islands, designated $y^i_{q,q'}$ (single collision):

$$y^i_{q,q'}(\text{corr})=y^i_{q,q'}-y^i_{q,q'}(DCB) \tag{A6}$$

The yields were then divided by the appropriate efficiencies and, for DI, IE, TI, and TE, multiplied by fac-

tors deduced from F_7 and F_8 to reflect the fractions of the yields due to the production of DI and IE or TI and TE. These factors can be shown to be simply the β_7 and β_8 defined in the previous paragraph. The resulting yields were then normalized to the target pressure P and multiplied by a single universal normalization factor N to give the final cross sections. The final expressions are

$$\sigma_{\rm SI} = y_{8,8}^2 N / (\epsilon P) , \tag{A7}$$

$$\sigma_{\rm DI} = y_{8,8}^1 N \beta_8 / (\epsilon_8 P) , \tag{A8}$$

$$\sigma_{\rm IE} = y_{8,8}^1 N (1 - \beta_8) / (\epsilon_8 P) , \tag{A9}$$

$$\sigma_{\rm SC} = y_{8,7}^2 ({\rm corr}) N / (\epsilon P) , \tag{A10}$$

$$\sigma_{\rm TI} = y_{8,7}^1 ({\rm corr}) N \beta_7 / (\epsilon_7 P) , \tag{A11}$$

$$\sigma_{\rm TE} = y_{8,7}^1 ({\rm corr}) N (1 - \beta_7) / (\epsilon_7 P) . \tag{A12}$$

[1]H. K. Haugen, L. H. Anderson, P. Hvelplund, and H. Knudsen, Phys. Rev. A **26**, 1962 (1982).

[2]H. Knudsen, L. H. Anderson, P. Hvelplund, G. Astner, H. Cederquist, H. Danared, L. Liljeby, and K. G. Rensfelt, J. Phys. B **17**, 3545 (1984).

[3]S. Datz, R. Hippler, L. H. Anderson, P. F. Dittner, H. Knudsen, H. F. Krause, P. D. Miller, P. L. Pepmiller, T. M. Rosseel, N. Stolterfoht, Y. Yamazaki, and C. R. Vane, Nucl. Instrum. Methods A **262**, 62 (1987).

[4]P. Richard, J. Hall, J. L. Shinpaugh, J. M. Sanders, T. N. Tipping, T. J. M. Zouros, D. H. Lee, and H. Schmidt-Böcking, Nucl. Instrum. Methods A **262**, 69 (1987).

[5]R. Gayet and A. Salin, J. Phys. B **20**, L571 (1987).

[6]R. E. Olson, J. Phys. B **12**, 1843 (1979).

[7]R. K. Janev and L. P. Presnyakov, J. Phys. B **13**, 4223 (1980).

[8]M. Glass-Maujean, K. Köllmann, and K. Ito, J. Phys. B **12**, L453 (1979).

[9]S. Arai, T. Yoshimi, M. Morita, K. Hironaka, T. Yoshlda, H. Koizumi, K. Shinsaka, and Y. Hatano, Z. Phys. D **4**, 65 (1986).

[10]S. Strathdee and R. Browning, J. Phys. B **9**, L505 (1976).

[11]R. M. Wood, A. K. Edwards, and M. F. Steuer, Phys. Rev. A **15**, 1433 (1977).

[12]K. E. Mcculloh and H. M. Rosenstock, J. Chem. Phys. **48**, 2084 (1968).

[13]F. B. Yousif, B. G. Lindsay, and C. J. Latimer, J. Phys. B **21**, 4157 (1988).

[14]A. K. Edwards and R. M. Wood, Phys. Rev. A **31**, 99 (1985).

[15]A. K. Edwards and R. M. Wood, Phys. Rev. A **34**, 4411 (1986).

[16]A. K. Edwards, R. M. Wood, A. S. Beard, and R. L. Ezell, Phys. Rev. A **37**, 3697 (1988).

[17]S. Cheng, E. Y. Kamber, C. L. Cocke, and S. L. Varghese, Nucl. Instrum. Methods B **40/41**, 47 (1989).

[18]R. M. Wood (private communication).

[19]J. Sanders (private communication).

[20]R. Shingal (private communication).

[21]L. Meng, C. O. Reinhold, and R. E. Olson, Phys. Rev. A **40**, 3637 (1989).

[22]R. Shingal, J. Phys. B **21**, 2065 (1988).

[23]M. Inokuti, Rev. Mod. Phys. **43**, 297 (1971).